Engineering Research Journal

journal homepage: https://erj.journals.ekb.eg/

Experimental Investigation of the Behaviour of Perforated Steel Cold-formed Column Encased in Lightweight Concrete

Omar M. Lotfy [1, *], Sameh M. Gaawan [1], and Mohamed M. Yehia [1]

[1] Civil Engineering Department, Faculty of Engineering at Mataria, Helwan University, 11718, Cairo, Egypt

[*]Corresponding Author E-mail: omar_lotfy@m-eng.helwan.edu.eg

Abstract

In recent years, cold-formed steel elements have been used more and more as primary load-bearing structures. The development of cost-effective structures is also a main concern in the field of structural engineering. That led to the combination of several materials to achieve this goal. This paper presents an experimental study conducted on cold-formed steel sections with perforations encased in lightweight concrete to investigate their behaviour during subjection to axial compression load. First, the material properties were determined from the tensile coupon test for steel used in cold-formed sections and standard cube/cylinder tests for lightweight concrete. Then, a total of twelve specimens were examined under the axial compression test, with two different cross-sections and various heights. The study's goals are to find out how lightweight encasement affects the behaviour and failure mode of the cold-formed steel column sections. Lightweight concrete encasement has greatly enhanced ultimate axial compression capacity, with a ratio ranging from 74.5–321.1% and 19.5–154.6% based on unit cost. Also, it enhanced the behaviour of cold-formed steel columns, eliminating distortional buckling failure mode and greatly restraining the lateral displacement of both the web and flanges of the cold-formed section. Furthermore, a comparison was conducted between international codes and test results to assess and estimate the behaviour and ultimate compression capacity of perforated bare steel and encased columns subjected to pure axial compression force.

Keywords: Cold-formed steel, Perforation, Encased, Lightweight concrete, Axial compression test, Ultimate compression capacity, and Experimental investigation.

DOI: 10.21608/erj.2024.377299
Received 14 May 2024; Received in revised form 23 May 2024; Accepted 8 July 2024
Available online 1 September 2024

1.Introduction

Designing economical buildings is essential in the field of structural engineering. As a result, cold-formed steel structures (CFS) and lightweight concrete were developed. Several papers investigate the behaviour of each material separately, but few of them investigate the composite effect between the CFS and lightweight concrete. CFS is widely used in commercial, residential, and industrial construction. By adding beneficial properties of lightweight concrete, such as insulation and fire protection, the composite structure will be cost-effective and environmentally friendly. In composite columns, composite action is essential to prevent the separation of thin steel sections from the concrete and to prevent local buckling that would otherwise lower the column's compressive strength. For this issue, a perforated CFS column section was chosen to enhance the shear bond between CFS and concrete. From a literature survey, the primary experimental investigations on composite CFS with concrete were reported.

Péter Hegyi [1] carried out an experiment test on a lipped cold-formed steel channel encased in polystyrene aggregate concrete (PAC) to examine the effect of different PAC mixtures on the compression capacity of the CFS as well as its effect on bracing the CFS. It was discovered that PAC was able to restrict global and distortional buckling and drove all specimens to fail owing to local buckling phenomena independent of CFS height. H. Taufiq [2] examined if the Eurocode (4) technique can be applied in the design of composite perforated channel CFS columns. The specimens consisted of a two-channel section forming a closed box section and were infilled with normal-weight concrete. The axial compression failure load was compared to Eurocode 4 (theoretical failure load), and it was found that there was a great agreement between the experimental failure load and Eurocode prediction. Jahid Ze-ghiche [3] investigated experimentally the behaviour of a fabricated CFS composite with normal-weight concrete, except that the natural gravel was substituted by crushed crystallized slag from a blast furnace. The CFS consists of two channels connected tip to tip, with two types of connection, either by discontinued weld along CFS edges or by continuous weld, and a stub height ranging from 50 to 500 mm. During the test of the 50 mm stub to estimate the non-buckling squash load for bare steel, it was discovered that the box section with discontinued weld had the least compressive capacity. While testing composite steel stubs, it was found that concrete can enhance steel compressive capacity by a ratio up to 3.12; similar results were found during the testing of the 500 mm stub.

The ultimate compression capacity of a built-up I-section consisting of two-lipped CFS channels connected back to back with self-drilling screw connectors composite with a ferro-cement jacket was experimentally investigated by Anis Saggaff [4]. The testing observation showed that the concrete jacket can enhance steel strength by up to 60% over bare steel, and the ferro-cement jacket was capable of providing lateral confinement to CFS and preventing local buckling failure mechanisms of CFS. Abubakar Sharif Auwalu [5] carried out an experiment test on lipped channel CFS connected back to back to form a built-up I-section and partially encased in ferro-cement to compare between partial

composite and bare CFS and to examine the structural behaviour of the column failure mode. The failure mode of the bare steel was discovered to be distortional buckling along the flanges and a little lip pop-out at the third end of the column. The composite column likewise experiences distortional and local buckling failure, and the ferro-cement explodes at the end of the test, the ultimate compressive strength of the composite column has increased by up to 160%.

Yue Li [6] investigated experimentally the behaviour of a fabricated box CFS composite with lightweight concrete under an axial compression test. The study uses four different types of lipped channel sections, and the test consists of 12 specimens divided into three configurations, double-limb, single-limb, and hollow specimens without lightweight concrete. Local buckling and concrete crushing were found to be the failure modes in all specimens. It was discovered that the filled concrete significantly increased the specimen's ultimate bearing capacity.

The behaviour and effectiveness of the CFS sections subjected to axial compression load under the influence of various cross-sections, perforated or non-perforated, stiffened or non-stiffened, composite with ordinary or lightweight concrete, were studied in previous research on the CFS column members. The majority of research on CFS columns concentrated on three types of sections: the first type is an infilled CFS tube section; the second type is an encased built-up I section consisting of two C-channels connected back to back; and the third type is an infilled built-up box section consisting of two C-channels connected tip to tip. Consequently, the purposes of this study are:

Studying the effect of lightweight concrete encasement on the behaviour and axial compression capacity of the CFS column consisting of single stiffened perforated C-sections experimentally.

So, experimentally tested the twelve CFS columns with bare CFS or composite with lightweight concrete, and with different dimensions subjected to axial compression. The results were used to achieve the objectives of this research.

2.Experimental Program

2.1. Specimens

A set of 12 specimens was tested to determine the behaviour of the CFS column under axial compression force. The test specimens were divided into two groups: the first group consisted of six bare CFS perforated columns, and the second group consisted of six CFS perforated columns encased in lightweight concrete. Each group contains two different CFS stiffened perforated channel sections with different lengths and dimensions. **Fig. (1)** illustrates CFS section dimensions and perforation shapes, locations, and dimensions, all in mm.

For group number two, the CFS is encased in lightweight concrete with a 30 mm all-around concrete cover. Before concrete mixing, two strain gauges with a 10 mm gauge

length were attached to the CFS columns' middle height, one at the middle web length and the other at the flange tip, for local axial strain measurements. CFS columns were installed in the wooden forms, and then lightweight concrete was poured. The vibrator was used to compact the concrete every 50 cm of concrete height for about 7 seconds only, to ensure that the concrete was fully compacted and to prevent lightweight concrete segregation due to excessive vibration. **Fig. (2)** shows the encased lightweight concrete column preparation and the detailed dimensions for the cross-section, all dimensions in mm.

Specimen labelling is conducted as follows: C-100-1.5-500-NE, where "C" stands for "column" and the numbers that follow "C" stand for the total web length of the CFS section, the plate thickness, and the specimen height, respectively. The letter "NE" denotes specimens that are not encased in lightweight concrete, whereas the letter "E" denotes specimens that are encased. The detailed section properties for each tested specimen are listed in **Table (1)**. The abbreviations listed in this table are: (W_w) means the overall web length, (W_f) means the flange width, (t) means thickness, (D x B) the concrete dimensions (depth x width) respectively, (H) the specimen height, (A_g) the gross area of steel cross-section, (A_n) the net area of steel cross-section, ($A_{concrete}$) the area of concrete cross-section, (r_{xg}) the gross radius of gyration in the x-direction for bare steel and modified radius of gyration for encased steel. Also, (r_{yg}) is the gross radius of gyration in the y-direction, and ($\lambda_{crtical}$) is the critical slenderness ratio (H/r).

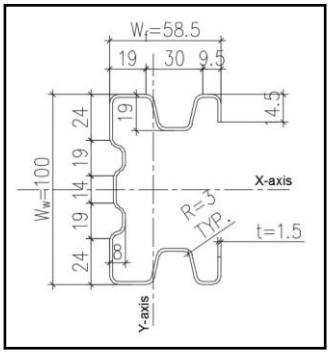

(a) C100-1.5 Section dimensions

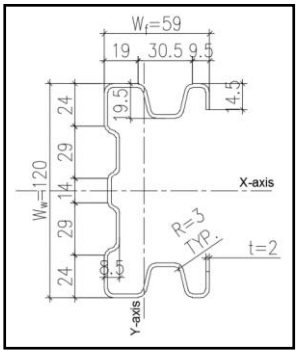

(b) C120-2 Section dimensions

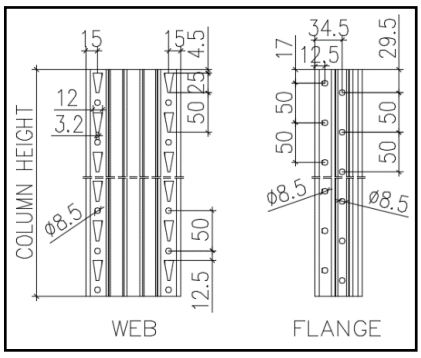

(c) Detailed perforation location on column web and flange

Fig. 1. Detailed dimensions for CFS column cross-sections

(a) Wooden forms for encased columns

(b) Compaction of encased column

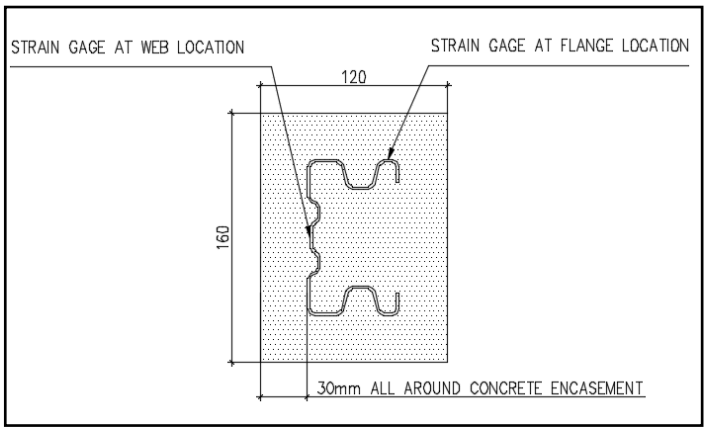

(c) C100-1.5 Encased column section dimensions

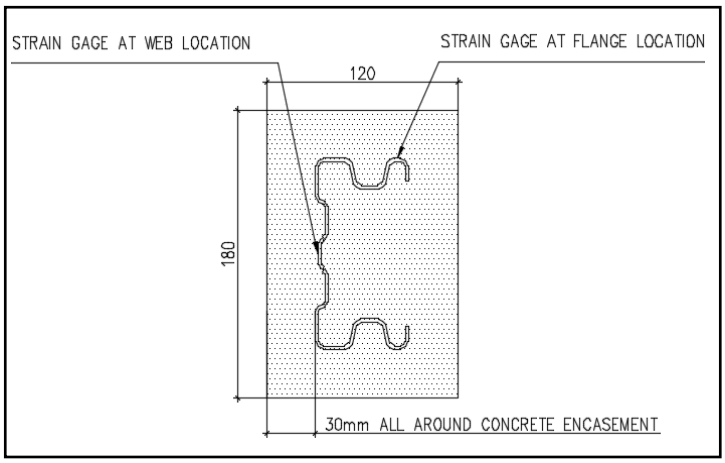

(d) C120-2 Encased column section dimensions

Fig. 2. Preparation and detailed dimensions for encased column

Table 1. Section properties of tested specimens

Specimen	W_w (mm)	W_f (mm)	t (mm)	DxB (Concrete) (mm x mm)	H (mm)	A_g (mm^2)	A_n (mm^2)	$A_{(concrete)}$ (mm^2)	r_{xg} (mm)	r_{yg} (mm)	$\lambda_{crtical}$
C100-1.5-500-NE	100	58.5	1.5	-	500	441.1	354.1	-	37.65	20.05	24.94
C100-1.5-1000-NE	100	58.5	1.5	-	1000	441.1	354.1	-	37.65	20.05	49.88
C100-1.5-2000-NE	100	58.5	1.5	-	2000	441.1	354.1	-	37.65	20.05	99.75
C120-2-500-NE	120	59	2	-	500	628.3	512.3	-	45.32	19.72	25.35
C120-2-1000-NE	120	59	2	-	1000	628.3	512.3	-	45.32	19.72	50.71
C120-2-2000-NE	120	59	2	-	2000	628.3	512.3	-	45.32	19.72	101.42
C100-1.5-500-E	100	58.5	1.5	160x120	500	441.1	354.1	19200	43.3	30.2	16.56
C100-1.5-1000-E	100	58.5	1.5	160x120	1000	441.1	354.1	19200	43.3	30.2	33.11
C100-1.5-2000-E	100	58.5	1.5	160x120	2000	441.1	354.1	19200	43.3	30.2	66.23
C120-2-500-E	120	59	2	180x120	500	628.3	512.3	21600	49.3	29.3	17.06
C120-2-1000-E	120	59	2	180x120	1000	628.3	512.3	21600	49.3	29.3	34.13
C120-2-2000-E	120	59	2	180x120	2000	628.3	512.3	21600	49.3	29.3	68.26

2.2. Material Properties

The virgin material of the steel sheets before the perforation and the cold-forming processes are S-355JR, with Fy equal to 355 MPa and Fu equal to 470 MPa. To determine the actual mechanical properties of CFS due to the cold forming process, a total of 14 tensile coupon tests were performed by a hydraulic Material Test System (MTS) machine. Seven coupons were cut from each cross-section C100-1.5, C120-2, consisting of three non-perforated flat coupons cut from the flat parts of the column web, two circle-perforated coupons cut from the flanges of the column, and two triangle-perforated coupons cut from the web of the column.

The load-elongation relationship was used to calculate the stress-strain relationship of tensile coupons. The material's ultimate tensile stress (Fu) was computed by dividing the failure ultimate load by the initial cross-sectional area (Pu/Ao). Based on the 0.2% offset strength method suggested by ASTM E8/E8M [11], the yield stress (Fy) was computed. The strain (Ɛ) was computed by dividing the elongation by the original gauge length of the test specimen (ΔL/Lo). Finally, the Young's modulus of each coupon (E= F/Ɛ) is computed by dividing the value of stress by the value of strain. Based on the average of the material properties for the seven coupons, the final material properties (Fu, Fy, and E) for each cross-section thickness are determined, as shown in **Table (2).**

The lightweight concrete mix was designed according to ACI 213R-14 [12], with mix proportions shown in **Table (3)**. The cement used in this research was Portland cement (CEM-I-42.5N), fine aggregate with a specific gravity equal to 2.63 and a fineness

modulus of 2.71, and Expanded Polystyrene Beads (EPS) with grain diameters ranging from 2 to 5 mm and a unit weight equal to 70 Kg/m3. The mix contains silica fume with a ratio equal to 10% of cement weight, superplasticizer (SP) with a ratio equal to 2% of cement weight, and water content to total cementitious material with a ratio of 0.35.

Three standard cylinders with dimensions of 150x300 mm and six standard cubes with dimensions of 150x150x150 mm were taken from the mix to conduct compression tests to determine the mechanical properties of lightweight concrete. The cubes were tested at the ages of 7 and 28 days to determine the average compressive strength and lightweight concrete density. The average cube compressive strength was 8 MPa at the age of 7 days and 9.32 MPa at the age of 28 days; the lightweight concrete density is 1400 kg/m3. The cylinders were tested at the age of 28 days to determine the average compressive strength and average modulus of elasticity of lightweight concrete. The average cylinder compressive strength of lightweight concrete is 8.77 MPa, and it was found to be around 94% of the 28-day cube strength. The average elasticity modulus of lightweight concrete is 8.5 GPa, and it was found to be in great agreement with the proposed model for the modulus of elasticity in [13].

Table 2. The average mechanical properties of the tensile coupon test results

Material thickness t (mm)	Non-perforated coupon			coupon has circular perforations from flange			coupon has triangular perforations from web			Final material properties		
	F_y (MPa)	F_u (MPa)	E (GPa)	F_y (MPa)	F_u (MPa)	E (GPa)	F_y (MPa)	F_u (MPa)	E (GPa)	F_y (MPa)	F_u (MPa)	E (GPa)
1.50	401	516.7	203.8	402.5	539.5	205.1	419	549.5	205.2	405	535	204.7
2.00	400	502	203.5	401	512.5	204.9	412.5	532.5	204.0	402.5	515	204.1

Table 3. Mixing proportions for lightweight concrete mix

CEMENT (kg/m3)	SILICA FUME (kg/m3)	WATER (L/m3)	SAND (kg/m3)	EPS (kg/m3)	SP (ml/Kg of cement)
400	40	155	650	40	2

2.3. Test Setup and Instrumentations

The test specimens were tested on a loading frame resting on a rigid floor consisting of eight girders divided into four top and bottom girders and four columns. All girders were connected with columns with bolted rigid connections. The distance between the floor's surface and the top of the loading frame is 3.1 m. The loading frame's capacity is 3000 kN,

and a hydraulic jack with a 1500 KN capacity and a 100 mm jack diameter was fastened to the loading frame girder's bottom flange, which was aligned with the loading system's centre for applying load to the test specimen as shown in **Fig. (3).**

A 35-mm-thick plate was used at the top and bottom of the specimens to ensure the uniformity of the load distribution on the specimen. The bottom base was unable to move vertically (Uz) due to the presence of the rigid loading frame girder and was unable to move in the horizontal direction (Ux, Uy) due to high friction between the specimen and the thick plate. The top of the specimen has the same boundary end condition except that it can move freely in the vertical direction (Uz). The same boundary conditions were used for encased steel columns, as shown in **Fig. (4)**. An extra column cap was installed at the top and bottom of the column to guarantee that the column ends faced an equal distribution of stress. The column cap consisted of 50x5 angles welded together to form a boundary box and was attached to the column by gypsum plaster.

Three dial gauges with 0.1 mm accuracy are connected to an LVDT system (Linear Variable Differential Transformers), as shown in **Fig. (4)**. They are used to calculate the displacements in each of the three dimensions (vertical, in-plane, and out-of-plane displacements) for each load incremental in mm. Dial gauges are located at the top of the column specimen, at the mid-height of the column flange's edge, and at the centre of the web. The axial shortening of the specimens was measured using the LVDT (ΔZ) readings, and the lateral displacements of the flange and web were measured using the LVDT (ΔX) and (ΔY) readings, respectively.

After column alignments and attaching dial gauges, the vertical loads were applied incrementally on the top of the column specimen. When the load applied to the specimen reached the failure point, the test was terminated. At each load increment, the LVDTs recorded the displacements through dial gauge readings. This procedure was performed repeatedly for each specimen, and a data acquisition system controlled all test data. All experimental tests were carried out in the laboratory of the faculty of engineering at Mattaria-Helwan University.

Fig. 3. Loading frame.

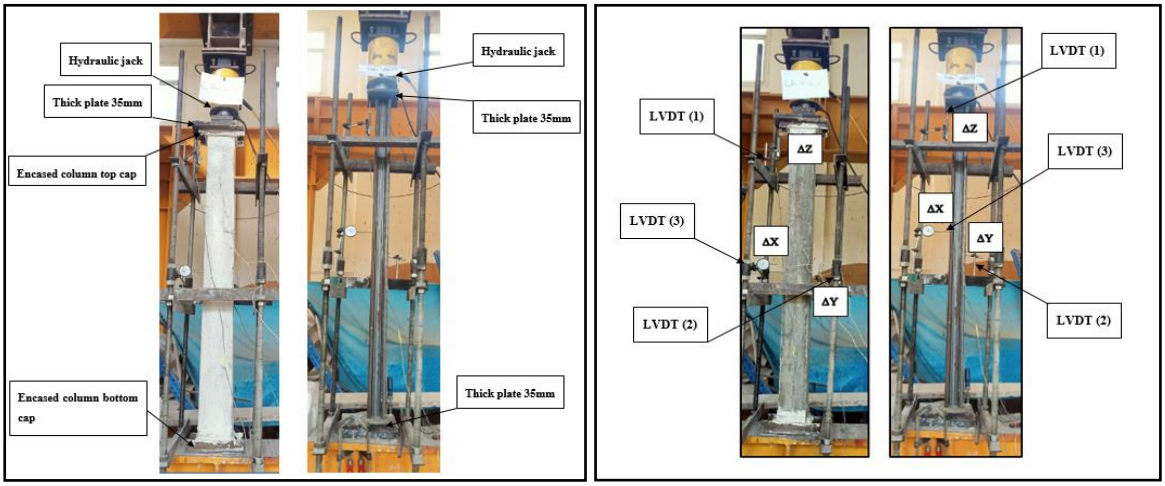

(a) Boundary condition of the specimens. **(b) Arrangement of LVDT.**

Fig. 4. Test setup and instrumentations

3. Test Results and Analysis

The axial compression test was conducted experimentally on twelve perforated specimens with two different cross-section dimensions and lengths, as detailed in **Table (1)**. The results of the ultimate failure load and the primary failure mode of the tested specimens are analyzed as follows:

3.1. Group Number One Results (Bare Steel Columns)

The failure mode of group number one depends on the height of the specimen, the behaviour of 500-mm-high columns and cross-sections C100-1.5-NE and C120-2-NE was governed by local and distortional buckling. The local buckling was concentrated at the centre of the web near the third end of the column, while distortional buckling happened at flanges in the middle of the column height. The behaviour of 1000 mm and cross-sections C100-1.5-NE, was governed by distortional buckling that happened at the middle of the column height. While, for cross-sections C120-2-NE, the behaviour was governed by both web-local and flange-distortional buckling that happened at the middle height of the column. The behaviour of 2000 mm and cross-sections C100-1.5-NE was governed by global flexural and distortional buckling. The buckling starts to happen about the column's weak axis at an earlier stage of loading, simultaneously with flange distortion. While, for cross-sections C120-2-NE, the behaviour was governed by flexural-torsional buckling with a large displacement of column web and flanges. **Fig. (5)** shows the influence of specimen height on buckling failure mode for specimens C100-1.5-NE and C120-2-NE.

Fig. (6-a) shows the load with axial shortening displacement curves for section type C100-1.5-NE. Comparing the results of the following specimens (C100-1.5-500-NE, C100-1.5-1000-NE, and C100-1.5-2000-NE) with different total heights and varying slenderness ratios (λcrtical), indicates that the specimen height has a great influence on the ultimate compression capacity of the bare cold-formed steel. The axial compression strength

decreased by 22.2% when the height increased from 500 mm to 1000 mm. Furthermore, increasing the specimen height from 1000 mm to 2000 mm resulted in a 47.1% loss in axial compression strength.

Fig. (6-b) shows the load with axial shortening displacement curves for section type C120-2-NE. Comparing the results of the following specimens (C120-2-500-NE, C120-2-1000-NE, and C120-2-2000-NE) with different total heights and varying slenderness ratios (λcrtical), indicates that the specimen height has a great influence on the ultimate compression capacity of the bare cold-formed steel. The axial compression strength decreased by 17.3% when the height increased from 500 mm to 1000 mm. Furthermore, increasing the specimen height from 1000 mm to 2000 mm resulted in a 35.2% loss in axial compression strength.

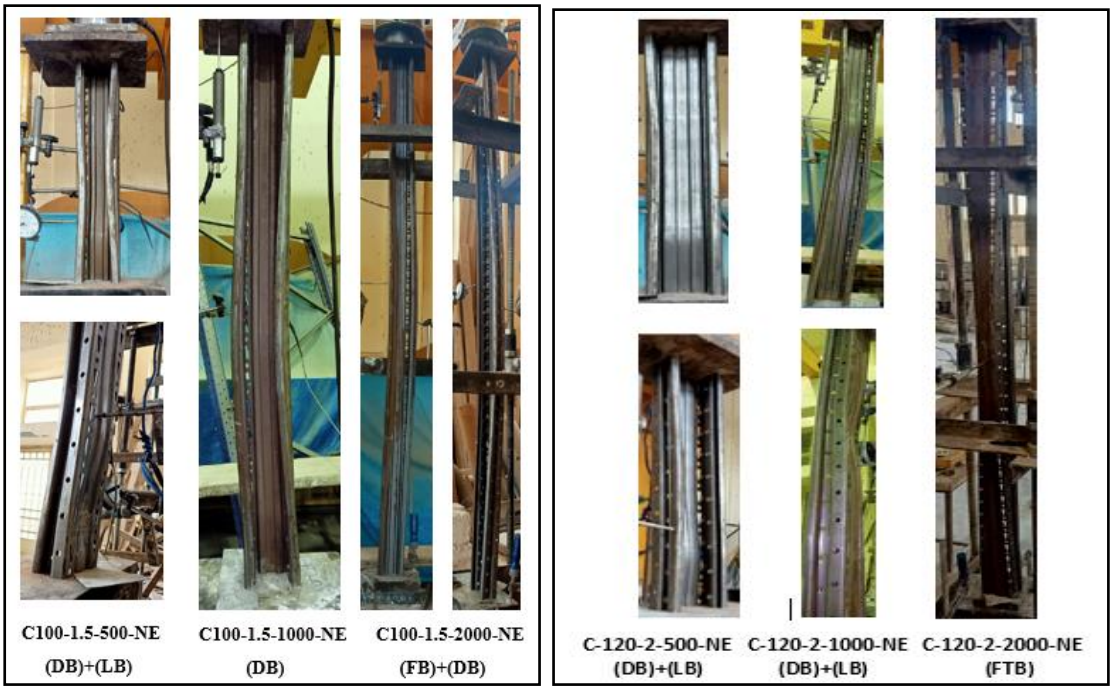

(a) Specimen C100-1.5-NE **(b) Specimen C120-2-NE**

Fig. 5. Buckling failure mode for group number one (bare-steel)

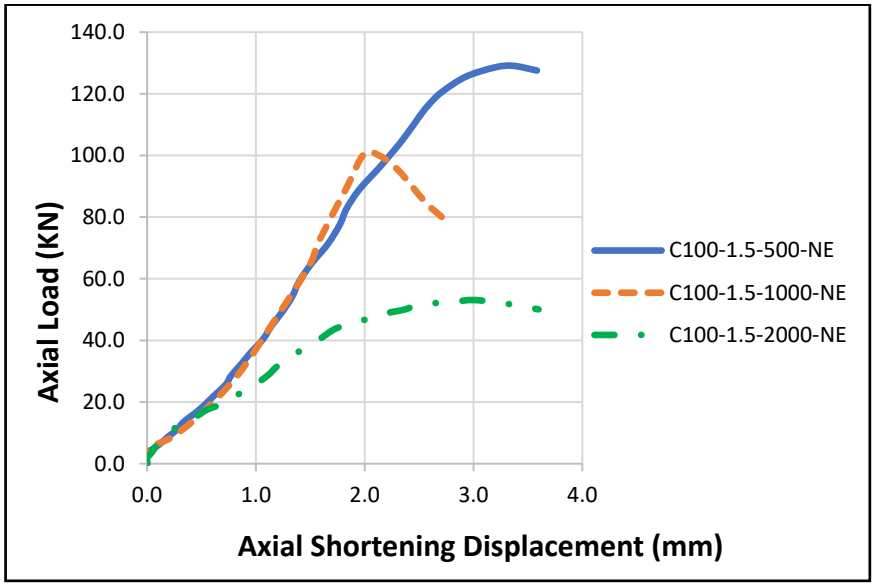

(a) Specimen C100-1.5-NE

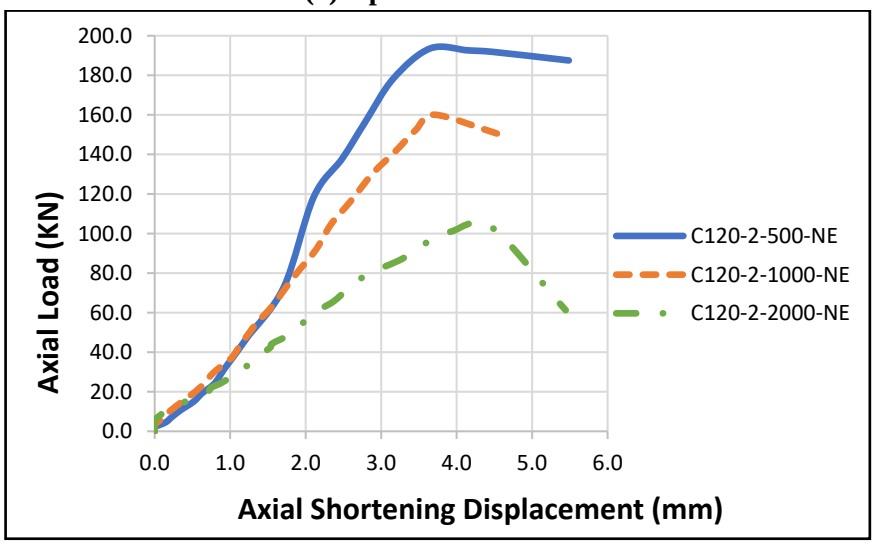

(b) Specimen C120-2-NE

Fig. 6. Load-axial shortening displacement for group number one (bare-steel)

3.2. Group Number Two Results (Encased Steel Columns)

The failure mode of group number two depends on the height of the specimen. The behaviour of 500-mm-high columns and cross-sections C100-1.5-E and C120-2-E was governed by concrete crushing. Cracks started to propagate at both ends of the column at 75% of the ultimate load, and vertical cracks at column flanges propagated prior to failure. The behaviour of 1000 mm and cross-sections C100-1.5-E and C120-2-E was governed by concrete crushing and web local buckling. For C100-1.5-E, vertical cracks started to propagate at the bottom end of the column at 80% of the ultimate load, and after removing the concrete encasement surrounding the CFS section and visual inspection, it was found

that there were few deformations at the CFS web and local buckling started to happen in the middle height of the column web. For C120-2-E, cracks started to propagate at the top end of the column at 65% of the ultimate load, and after removing the concrete encasement surrounding the CFS section and visual inspection, it was found that there were excessive deformations at the CFS web and local buckling (LB) happened at the top height of the column web. The behaviour of 2000 mm and cross-sections C100-1.5-E and C120-2-E was governed by global flexural buckling; the buckling starts to happen about the column's weak axis before failure. **Fig. (7)** shows the influence of specimen height on buckling failure mode for specimens C100-1.5-E and C120-2-E.

Fig. (8-a) shows the load with axial shortening displacement curves for section type C100-1.5-E. Comparing the results of the following specimens (C100-1.5-500-E, C100-1.5-1000-E, and C100-1.5-2000-E) with different total heights and varying slenderness ratios (λcrtical), indicates that the specimen height has little influence on the ultimate compression capacity of the encased cold-formed steel. The axial compression strength decreased by 9.8% when the height increased from 500 mm to 1000 mm. Furthermore, increasing the specimen height from 1000 mm to 2000 mm resulted in a 10.8% loss in axial compression strength.

Fig. (8-b) shows the load with axial shortening displacement curves for section type C120-2-E. Comparing the results of the following specimens (C120-2-500-E, C120-2-1000-E, and C120-2-2000-E) with different total heights and varying slenderness ratios ($\lambda_{crtical}$), indicates that the specimen height has little influence on the ultimate compression capacity of the bare cold-formed steel. The axial compression strength decreased by 11.7% when the height increased from 500 mm to 1000 mm. Furthermore, increasing the specimen height from 1000 mm to 2000 mm resulted in a 7.8% loss in axial compression strength.

The load-strain curve extracted from the strain gauge for the web mid-height and the strain gauge of the flange tip is illustrated in **Fig. (9)**. For C100-1.5-E and 500 mm specimens, the web strain reached up to 94% from yield stress. While for 1000 mm and 2000 mm, smaller values reached up to 75% from web yield stress and 65% from flange stress. For C120-2-E and 500 mm specimens, they reached similar values as C100-1.5-NE. For 1000 mm and 2000 mm specimens, 87% and 93% of web yield stress were reached, respectively, and 85% and 68% of flange yield stress were reached, respectively.

3.3. The Normalized Ultimate Compression Strength Ratio

The ratio between the maximum value of the axial failure load ($P_{u(exp)}$), as determined by the experimental test, and the axial yield load (P_y) for each specimen is known as the normalized ultimate compression strength ratio. P_y computed for bare steel as follows ($F_y \times A_n$), while for encased steel, ($F_y \times A_n + F_{cu'} \times (A_{concrete} - A_n)$).

Table (4) shows that the values of the normalized ultimate compression strength ratio ($P_{u(exp)}/P_y$) for all specimens ranged from 0.30 to 0.94 according to the value of the slenderness and compactness ratio. For all long column encased steel specimens, the

normalized ultimate compression ratio exceeds that of bare steel. This is because of the significant influence of lightweight concrete composite action with CFS. The abbreviations listed in this table for failure mode are (LB) local buckling, (DB) distortional buckling, (FB) flexural buckling, and (FTB) flexural torsional buckling.

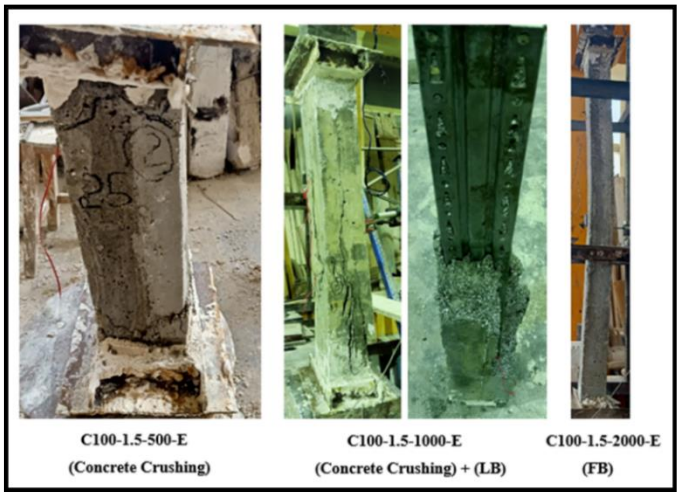

(a) Specimen C100-1.5-E

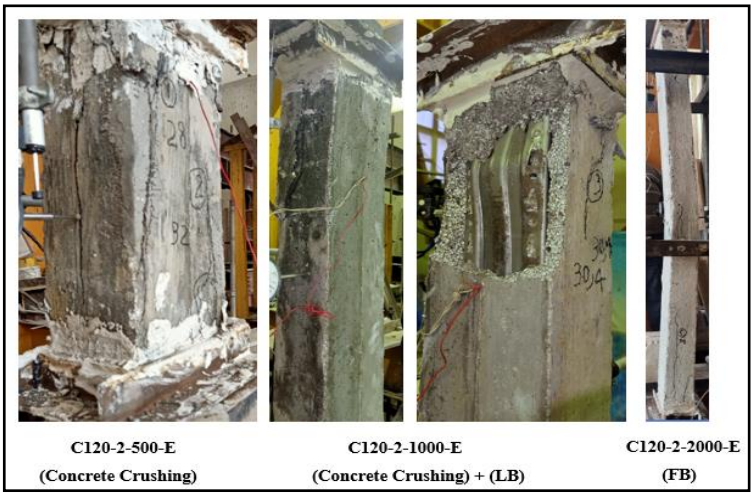

(b) Specimen C120-2-E

Fig. 7. Buckling failure mode for group number two (encased steel)

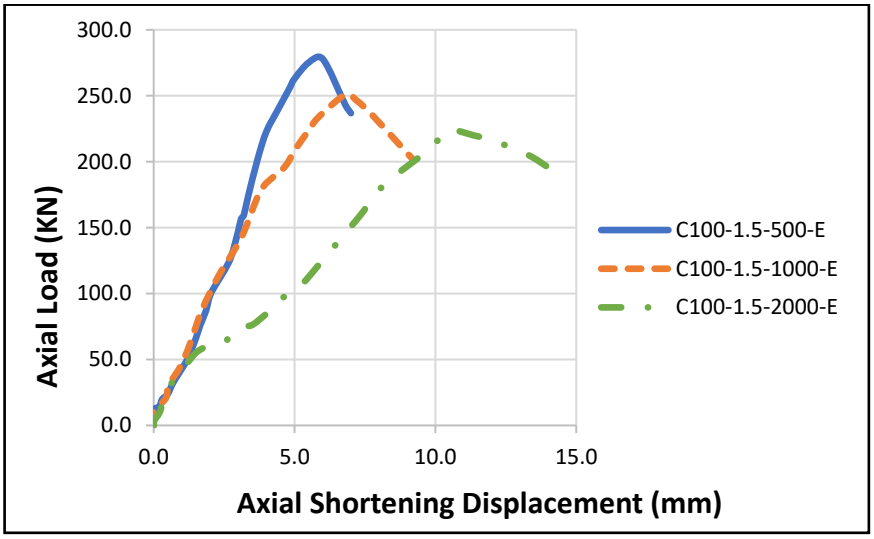

(a) Specimen C100-1.5-E

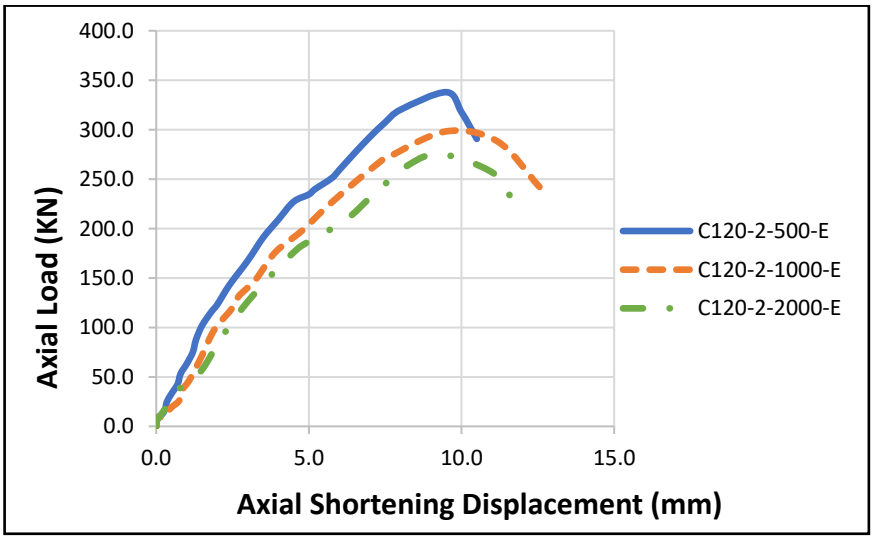

(b) Specimen C120-2-E

Fig. 8. : Load-axial shortening displacement for group number two (encased steel)

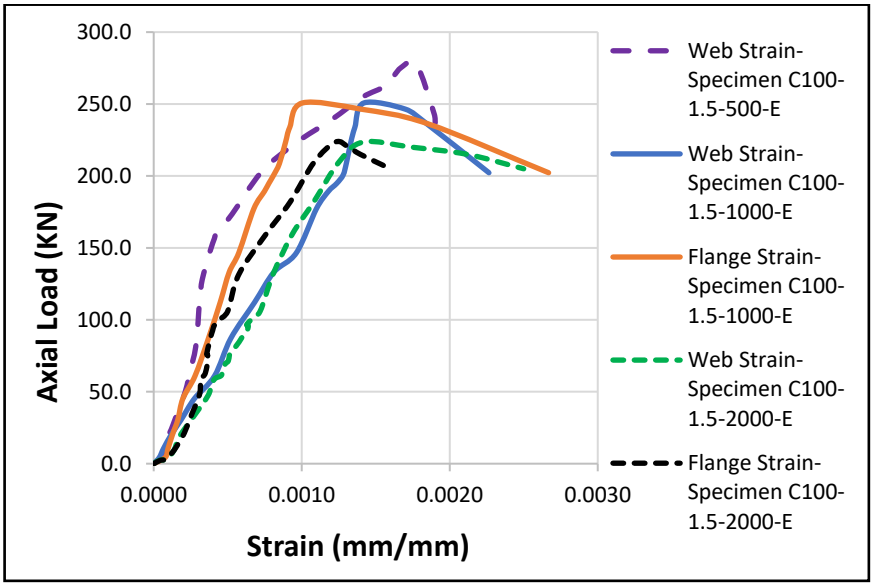

(a) Specimen C100-1.5-E

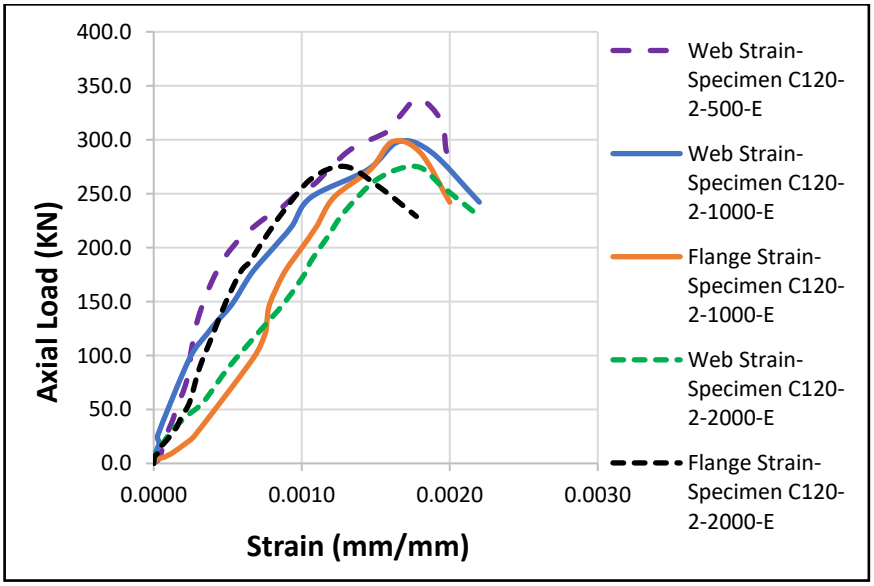

(b) Specimen C120-2-E

Fig. 9. : Load-strain curves for group number two (encased steel)

Table 4. Compression ultimate capacity and failure mode for all test specimens

Specimen	W_w/t	W_f/t	$\lambda_{crtical}$	$P_{u(exp)}$ (kN)	P_y (kN)	$\frac{P_{u(exp)}}{P_y}$	Failure mode
C100-1.5-500-NE	66.67	39	24.94	129.10	143.4	0.90	DB+LB
C100-1.5-1000-NE	66.67	39	49.88	100.36		0.70	DB
C100-1.5-2000-NE	66.67	39	99.75	53.10		0.37	DB+FB
C120-2-500-NE	60	29.5	25.35	193.60	206.2	0.94	DB+LB
C120-2-1000-NE	60	29.5	50.71	160.07		0.78	DB+LB
C120-2-2000-NE	60	29.5	101.42	103.66		0.50	FTB
C100-1.5-500-E	66.67	39	16.56	277.96	308.7	0.90	Concrete Crushing
C100-1.5-1000-E	66.67	39	33.11	250.78		0.81	Concrete Crushing+LB
C100-1.5-2000-E	66.67	39	66.23	223.59		0.72	FB
C120-2-500-E	60	29.5	17.06	337.93	391.2	0.86	Concrete Crushing
C120-2-1000-E	60	29.5	34.13	298.29		0.76	Concrete Crushing+LB
C120-2-2000-E	60	29.5	68.26	275.17		0.70	FB

3.4. The Influence of Lightweight Concrete Encasement for Steel Columns

For C100-1.5 and C120-2, the lightweight concrete encasement greatly affects the ultimate compression capacity of the section. For a 500-mm specimen length, the concrete encasement enhances the axial compression strength by 115.4% for the C100-1.5 section and 74.5% for the C120-2 section. For a 1000-mm specimen length, the encasement increases the axial compression capacity by 149.9% for the C100-1.5 section and 86.3% for the C120-2. For a 2000-mm specimen length, the encasement increases the axial compression capacity by 321.1% for the C100-1.5 section and 165.5% for the C120-2. The effect of the encasement increases while increasing the length of the specimen, and for less stiff CFS (C100–1.5), the effect of the encasement is larger than that of stiffer C120–2. For optimum values of CFS stiffness encased with concrete, further numerical and experimental investigations need to be conducted.

Fig. (10) shows the effect of concrete encasement on the lateral displacement of the web and flanges for the CFS. For all specimens, the value of web and flange displacement is small for encased specimens compared with bare CFS. That's because of the lateral confinement of the lightweight concrete; except for the 2000 mm specimen, the web displacement is nearly the same due to flexural buckling around the minor column axis.

Fig. (11) shows the typical failure mode for bare and encased CFS. The lightweight concrete encasement greatly restrains the local and global buckling phenomena of CFS. For a 500-mm specimen length, the encasement eliminated the local and distortion

buckling phenomena. For 1000 mm, the distortion buckling was eliminated, but the local buckling happened in the specimen, as shown in **Section 3.2**. For 2000 mm, distortional and flexural-torsional buckling phenomena were eliminated, and the specimens failed due to global flexural buckling.

A comparison depending on cost was conducted to compare the additional costs added by extra-lightweight concrete encasement to the bare CFS. According to the Egyptian construction market for the year (2023) the price of CFS sheets is 50,000 L.E. per ton, and for ready-mix lightweight concrete, the price of 1 m^3 is 5,000 L.E. For the percentage increase in the ultimate capacity, taking into account the increase in specimen cost, the following equation will be used:

$$\frac{\frac{\mathbf{Pu_{c-E}}}{\mathbf{Specimen\ cost}} - \frac{\mathbf{Pu_{c-NE}}}{\mathbf{Specimen\ cost}}}{\frac{\mathbf{Pu_{c-NE}}}{\mathbf{Specimen\ cost}}}$$

For a 500-mm specimen length, the percentage increase in ultimate capacity based on cost is 36.1% for the C100-1.5 section and 19.5% for the C120-2. For 1000 mm, the percentage increase in ultimate capacity based on cost is 58% for the C100-1.5 section and 27.6% for the C120-2. For 2000 mm, the percentage increase in ultimate capacity based on cost is 154.6% for the C100-1.5 section and 81.7% for the C120-2. The effect of the encasement cost increases while increasing the length of the specimen, and for a smaller area of CFS (C100-1.5), the effect of the encasement is larger than that of C120-2. For the optimum values of the CFS area encased in concrete, further numerical and experimental investigations need to be conducted.

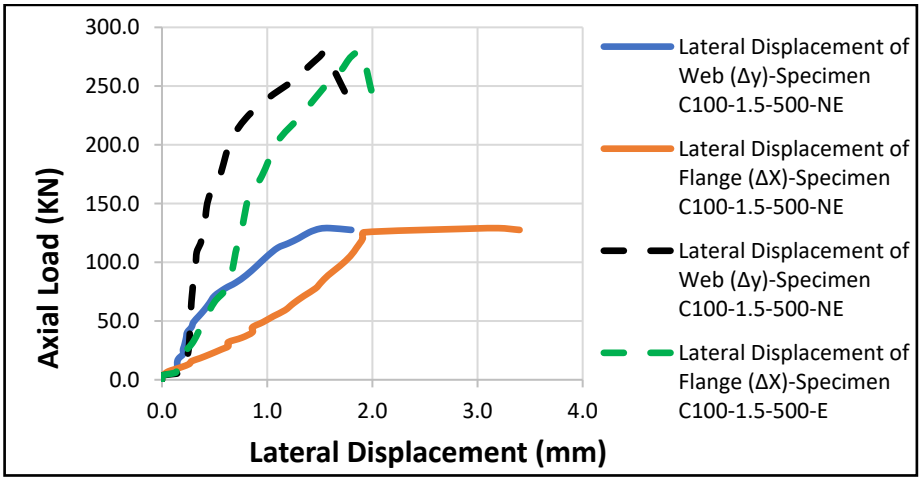

(a) Specimen C100-1.5-500

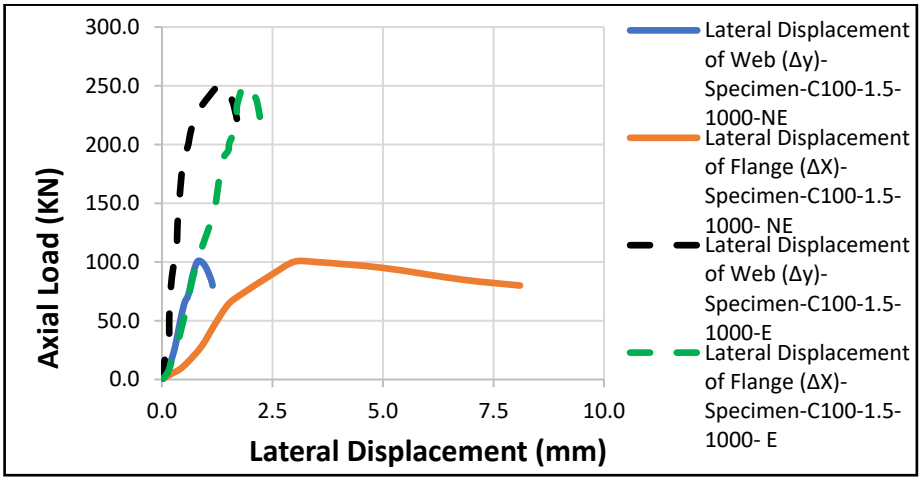

(b) Specimen C100-1.5-1000

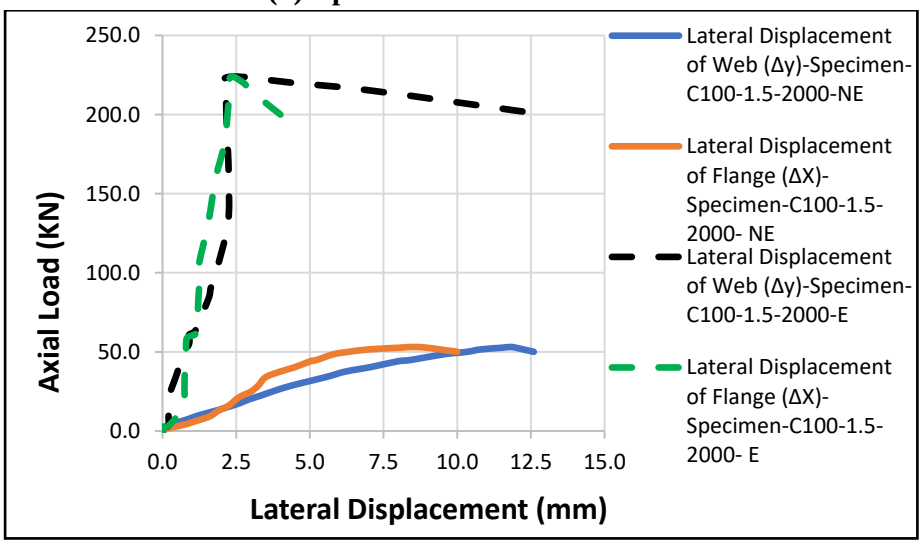

(c) Specimen C100-1.5-2000

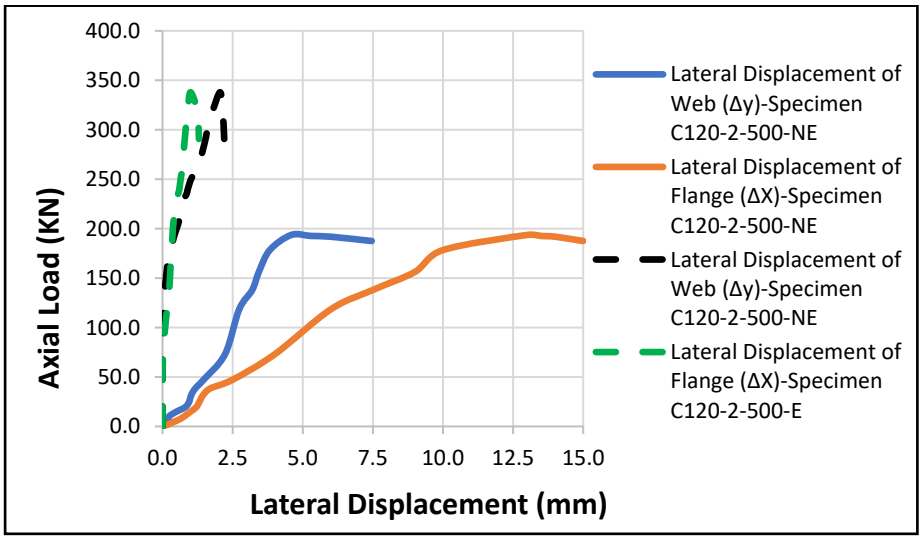

(d) Specimen C120-2-500

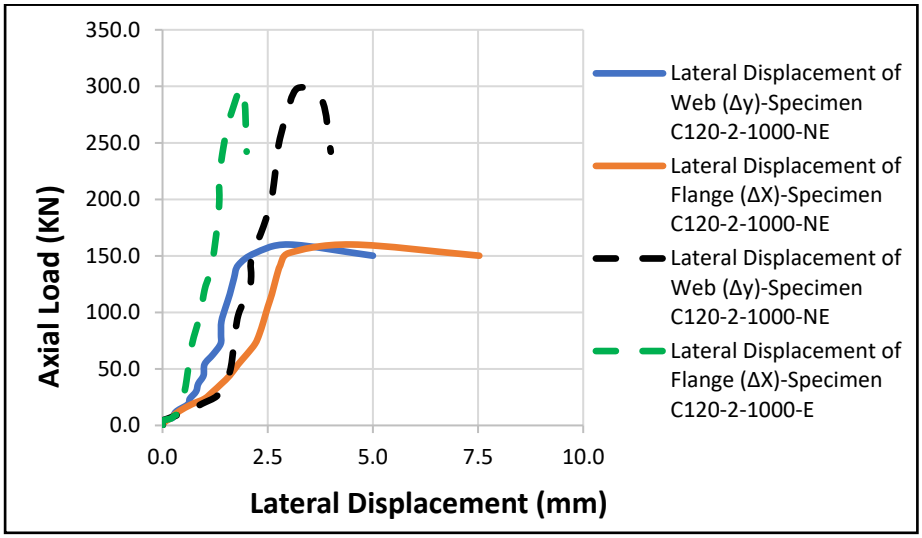

(e) Specimen C120-2-1000

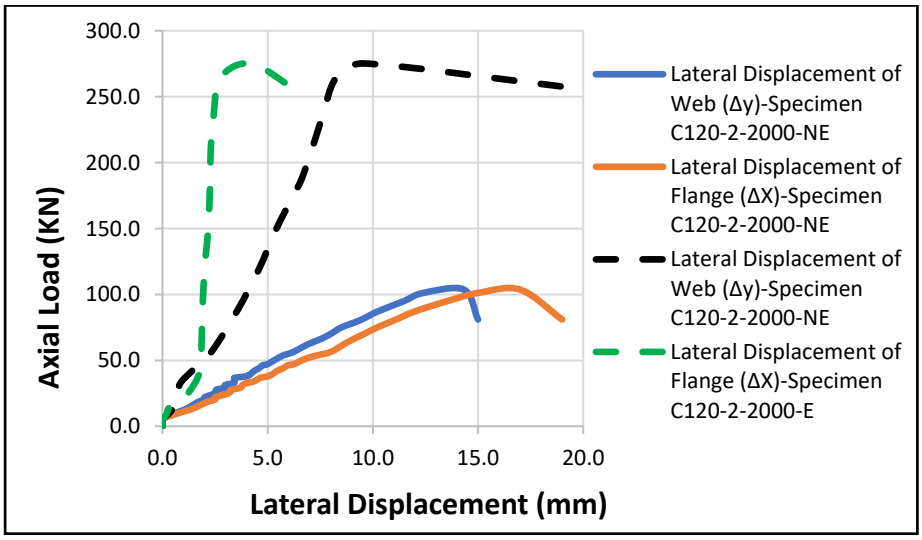

(f) Specimen C120-2-2000

Fig. 10. Load-lateral displacement curve for the influence of lightweight concrete encasement

(a) Specimen C100-1.5-500

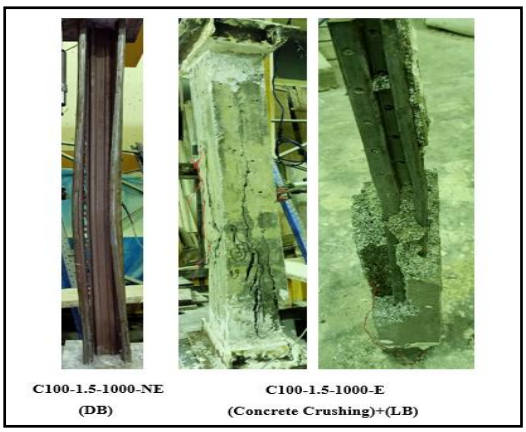

(b) Specimen C100-1.5-1000

(c) Specimen C100-1.5-2000

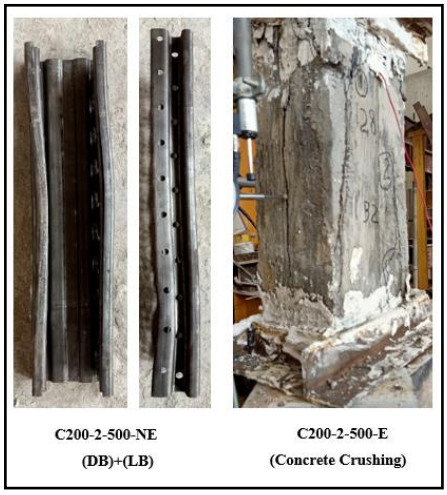

(d) Specimen C120-2-500

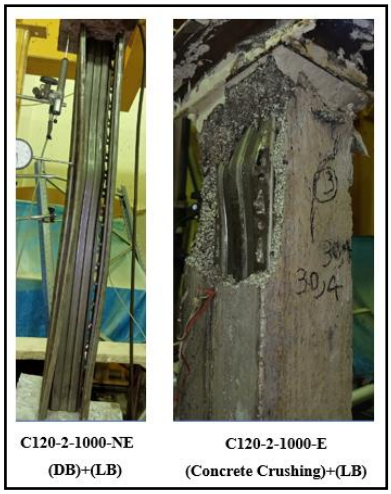

(e) Specimen C120-2-1000

(f) Specimen C120-2-2000

Fig. 11. Typical failure mode for bare and encased CFS

4.Comparison between International Codes Methods and Experimental Test

This section investigates the applicability of using international codes such as AISI-S100 [9], AISC360 [10], and Eurocode 4, 3, [7], [8] to assess and estimate the behaviour and ultimate compression capacity of perforated bare steel and encased columns subjected to pure axial compression force.

4.1. Group number one (Bare steel Columns) and (AISI-S100, Eurocode 3) comparison

A comparison between group number one bare steel CFS columns and (AISI-S100 [9] and Eurocode (3) [8]) is conducted based on the ultimate compression failure load and the expected failure mode.

AISI standards it is based on the direct analysis method (DSM) and can expect local, distortion, global flexural and flexural torsional buckling failure loads. The average properties used to calculate the equivalent slenderness parameter (λ_c, λ_L, λ_d) for flexural (F_{cre}) and flexural-torsional buckling critical stress (F_e), local buckling critical stress (F_{crl}), and distortional buckling critical stress (F_{crd}) are first calculated for all CFS sections, accounting for the effect of perforations. The buckling load is then calculated using the gross area (A_g) of the CFS section.

Table (5) illustrates the comparison between the experimental test load ($P_{u,\ Test}$) and the theoretically calculated value for ultimate compression axial force ($P_{n,\ AISI}$), which is the minimum between flexural, flexural torsional, local, and distortional buckling ultimate loads. It is clear that AISI didn't expect the correct failure mode in all specimens except for C120-2-2000-NE, and the local buckling mode is the governing mode in short and intermediate specimens. As the specimen height/slenderness ratio increases, the theoretical calculations are conservative for the estimation of the ultimate load; however, at short specimens, the ultimate compression load was in excellent agreement. For ultimate compression load, the ratio between the test and AISI standard ranges from 1.11 to 1.69, depending on specimen height.

Eurocode (3) standards are based on the effective width/area method used to compute the effective area of the CFS and then estimate the failure load for global flexural and flexural torsional buckling loads only. The influence of intermediate stiffeners and perforations is taken into consideration when computing the effective width of all CFS sections. For all cross-sections, all elements are determined to be fully effective. The non-dimensional slenderness parameter ($\bar{\lambda}, \bar{\lambda}_T$) for both flexural and flexural-torsional buckling is estimated using the effective area (A_e). The reduction factor (χ) is then computed using the buckling curve (C), and the buckling load is calculated using the net area (A_n) of the CFS section.

Table (5) illustrates the comparison between the experimental test load (Pu, Test) and the theoretically calculated value for ultimate compression axial force ($P_{n,\ En(3)}$), which is the minimum between flexural buckling and flexural torsional buckling ultimate load. It is clear that Eurocode didn't expect the correct failure mode in all specimens except for C120-2-2000-NE. This is due to the fact that there is no estimation for the local and distortional buckling failure modes at EN standards. As the specimen height/slenderness ratio increases, the theoretical calculations are conservative for the estimation of the ultimate load; however, at short specimens, the ultimate compression load was in excellent agreement. For ultimate compression load, the ratio between the test and EN standard varies from 1.05 to 1.67 depending on specimen height.

Table 5. Comparison between Euro code (3), AISI Standards and Test Results of Bare Steel for all Test Specimens

Specimen	($P_{u,\ Test}$) (kN)	($P_{n,\ AISI}$) (kN)	($P_{n,\ En(3)}$) (kN)	$\frac{P_{u,Test}}{P_{n,AISI}}$	$\frac{P_{u,Test}}{P_{n,En(3)}}$	Test Failure mode	AISI Theoretical Failure mode	Eurocode 3 Theoretical Failure mode
C100-1.5-500-NE	129.10	114.92	122.84	1.12	1.05	DB+LB	LB	FTB
C100-1.5-1000-NE	100.36	86.20	82.89	1.16	1.21	DB	LB	FTB
C100-1.5-2000-NE	53.10	31.37	34.82	1.69	1.52	DB+FB	FTB	FTB
C120-2-500-NE	193.60	174.32	182.26	1.11	1.06	DB+LB	LB	FTB
C120-2-1000-NE	160.07	140.95	132.31	1.14	1.21	DB+LB	LB	FTB
C120-2-2000-NE	103.66	61.99	62.12	1.67	1.67	FTB	FTB	FTB

4.2. Group number two (Encased steel Columns) and (AISC360-16, Eurocode 4) comparison

A comparison between group number two CFS columns encased in lightweight concrete and (AISC360 [10], Eurocode (4) [7]) is conducted based on the ultimate compression failure load and the expected failure mode.

AISC-360 standards were used for computing the ultimate compression load. The code estimated the ultimate strength based on modified properties of the composite section for global buckling behaviour and eliminated the local and distortion buckling failure mechanisms. However, the AISC code states some requirements are mandatory for using code procedures for the design of the encased steel sections that are not applicable to the conducted test cases, such as the presence of longitudinal reinforcement bars and lateral ties, and the steel section should be double-symmetric. The effective stiffness (E_{Ieff}) for all CFS sections was computed, then the ultimate squash load (P_{no}) and the elastic critical buckling load (P_e) were computed, and then the ultimate compression axial load (P_n) was computed from the steel net section area (A_n).

Table (6) illustrates the comparison between the experimental test load ($P_{u,\ Test}$) and the theoretically calculated value for ultimate compression axial force ($P_{n,\ AISC}$). It is clear that AISC didn't expect the correct failure mode in all specimens except for 2000 mm specimens. Depending on the specimen height, the ratio between the test and AISC standard for ultimate compression load varies from 0.93 to 1.29. For short and intermediate columns, the theoretical calculations overestimate the ultimate load, whereas, for long column specimens, they are conservative.

Eurocode (4) standards were used for computing the ultimate compression load. The code estimated the ultimate strength based on modified properties of the composite section for global buckling behaviour and eliminated the local and distortion buckling failure mechanisms. However, the Eurocode states some requirements are mandatory for using

code procedures for the design of the encased steel sections, which are not applicable to the test cases conducted, such as that the characteristic cube strength of normal weight concrete must be greater than 20 MPa and the steel section should be a double-symmetric section. The plastic resistance to compression ($N_{pl,\ Rd}$) and the effective flexure stiffness (E_{Ieff}) are computed to determine the non-dimensional slenderness parameter ($\bar{\lambda}$) for global buckling, and then the buckling curve (C) is used to compute the reduction factor (χ) to determine the buckling load based on the net area (A_n) of the CFS section.

Table (6) illustrates the comparison between the experimental test load ($P_{u,\ Test}$) and the theoretically calculated value for ultimate compression axial force ($P_{n,\ En(4)}$). It is clear that Eurocode (4) didn't expect the correct failure mode in all specimens except for 2000 mm specimens. Depending on the specimen height, the ratio between the test and Eurocode for the ultimate compression load varies from 0.94 to 1.26. For short and intermediate columns, the theoretical calculations overestimate the ultimate load, whereas, for long column specimens, they are conservative.

Table 6. Comparison between Euro code (4), AISC Standards and Test Results of Encased Steel for all Test Specimens.

Specimen	($P_{u,\ Test}$) (kN)	($P_{n,\ AISC}$) (kN)	($P_{n,\ En(4)}$) (kN)	$\frac{P_{u,Test}}{P_{n,AISC}}$	$\frac{P_{u,Test}}{P_{n,En(4)}}$	Test Failure mode	AISC Theoretical Failure mode	Eurocode 4 Theoretical Failure mode
C100-1.5-500-E	277.96	275.23	281.64	1.01	0.99	Concrete Crushing	FB	FB
C100-1.5-1000-E	250.78	250.77	250.03	1.00	1.00	Concrete Crushing+ LB	FB	FB
C100-1.5-2000-E	223.59	172.83	176.91	1.29	1.26	FB	FB	FB
C120-2-500-E	337.93	352.11	358.96	0.96	0.94	Concrete Crushing	FB	FB
C120-2-1000-E	298.29	320.29	316.76	0.93	0.94	Concrete Crushing+ LB	FB	FB
C120-2-2000-E	275.17	219.3	218.89	1.25	1.26	FB	FB	FB

5. Conclusions

This paper has presented an experimental study on CFS sections with perforations to investigate the CFS behaviour subjected to axial compression load. A total of twelve experimental results were reported; the material properties were determined from the tensile coupon test and standard cube/cylinder tests; and the failure modes along with axial capacity, load-axial shortening, and load-lateral displacement relationships were discussed. The investigation focused on the effects of thickness, overall web length of cross-sections, column total heights, and the effect of lightweight concrete encasement.
Based on the experimental results and the comparison between international standards presented in this paper, the following conclusions are drawn:

1. The range of the normalized ultimate compression strength ratio (ultimate test strength/yield strength) ($P_{u(test)}/P_y$) was 0.37 to 0.94, and for all long column-encased steel specimens, the normalized ultimate compression ratio exceeded that of bare steel. This led to the conclusion that lightweight concrete composites have a significant influence on CFS.
2. For bare cold-formed steel specimens with total heights of 500 and 1000 mm, the test results indicated that the interaction between distortional and local buckling is the main governing failure mode. For specimens with a total height of 2000 mm, the failure mode depends on the cross-section of steel. For C100, the governing failure mode is the interaction between distortional and global flexural buckling, and for C120, the governing failure mode is flexural torsional buckling.
3. For the encased steel, the encasement eliminates the distortional buckling mode for all test specimen heights and eliminates local buckling for short columns, while for long columns, the global flexural buckling is the main governing failure mode.
4. The influence of specimen height on bare cold-formed steel specimens was investigated, and it was found that the ultimate axial compression capacity was reduced by approximately 17.3 to 22.2% when the specimen height doubled from 500 to 1000 mm. Furthermore, when the specimen height doubled from 1000 to 2000 mm, the ultimate axial compression capacity was reduced by a ratio ranging from 35.2 to 47.1%. It is clear that specimen height has a significant effect on the ultimate axial compression capacity for bare steel.
5. The influence of specimen height on encased steel specimens was investigated, and it was found that the ultimate axial compression capacity was reduced by approximately 9.8 to 11.7% when the specimen height doubled from 500 to 1000 mm. Furthermore, when the specimen height doubled from 1000 to 2000 mm, the ultimate axial compression capacity was reduced by a ratio ranging from 7.8 to 10.8%. It is clear that the specimen height has a very minor effect on the ultimate axial compression capacity of the encased steel.
6. The influence of lightweight concrete encasement on the ultimate axial compression capacity ranges from 74.5 to 321.1%. For the lesser stiffness CFS core (C100), the

encasement has a much greater influence than the stiffer core (C120); however, both CFS cores have a significant enhancement in ultimate compression capacity, the ratio of enhancement increases while the specimen height increases, the lateral displacements for both the flange and the web of the cross-section have greatly improved by the confinement of the lightweight concrete encasement.

7. The influence of lightweight concrete encasement on the ultimate axial compression capacity ranges from 19.5 to 154.6%. Compared to the increase in specimen cost, the ratio of enhancement increases while the specimen height increases.
8. AISI-S100 and Eurocode (3) didn't expect the correct failure mode for the majority of bare cold-formed steel; however, for short and intermediate columns, it has a good agreement in predicting the failure load, but for long columns, it is very conservative in prediction.
9. AISC-360 and Eurocode (4) didn't expect the correct failure mode for the majority of encased steel; however, for short and intermediate columns, it overestimated in predicting the failure load, but for long columns, it was conservative in prediction.

References

1. Péter Hegyi, László Dunai. (2016), "Experimental Investigations on Ultra-Lightweight-Concrete Encased Cold-Formed Steel Structures, PartII: Stability Behaviour of Elements Subjected to Compression," Thin-Walled Structures, no. 101 (2016) 100-108.
2. H. Taufiq, R.M. Lawson. (2020), "Composite Columns Using Perforated Cold Formed Steel Sections," Journal of Constructional Steel Research, no. 167-105935.
3. Jahid Zeghiche. (2013), "Further Tests on Thin Steel and Composite Fabricated Stubs," Journal of Constructional Steel Research, no. 81 124-137
4. Anis Saggaff, Khaled Alenezi, Mahmood Md Tahir, Talal Alhajri, Mohamad Ragae. (2015), "Behaviour of Composite Column of Cold-formed Steel Section without Web Stiffener Integrated with Ferro-cement Jacket," Applied Mechanics and Materials, no. 752-753 pp 528-532.
5. Abubakar sharif Auwalu, Abdul Kadir Marsono, Mahmood Md Tahir, Arizu Sulaiman. (2020), "Behaviour of Cold-Formed Ferrocement Composite Column under Axial Loading," Journal of Critical Reviews, vol. 7, no. 2394-5125
6. Yue Li, Yong Yan, Xue Meng, Kechao Zhang, Xiaorun Li, Chongming Gao. (2022), "Experimental Study on Axial Compression Performance of Thin-Walled Steel Tube Lightweight Concrete Columns with Composite Section," Frontiers in Materials, vol. 9.
7. EN 1994-1-1 (2022). Eurocode 4, Design of composite steel and concrete structures-Part 1-1, General rules and rules for buildings.
8. EN 1993-1-1 (2022). Eurocode 3, Design of steel structures-Part 1-1, General rules and rules for buildings.

9. AISI-S100. (2016). North American Specification for the Design of Cold-Formed Steel Structural Members, American Iron, and Steel Institute, Washington, D.C.
10. AISC 360-22 (2022). American Institute of Steel Construction, Specification for Structural Steel Buildings, Washington, D.C.
11. ASTM E8/E8M-16a, (2016). Standard Test Methods for Tension Testing of Metalic Materials.
12. ACI 213R-23 (2023) Guide for Structural Lightweight- Aggregate Concrete
13. V. Behnam and N. Shami, (2017). "Review on the Mixture Design and Mechanical Properties of the Lightweight Concrete Containing Expanded Polystyrene Beads," Australian Journal of Structural Engineering, no. 1328-7982.